

Contents lists available at [SciVerse ScienceDirect](http://SciVerse.ScienceDirect.com)

## Physics Letters B

[www.elsevier.com/locate/physletb](http://www.elsevier.com/locate/physletb)The  $A(K_{stop}^-, \pi^\pm \Sigma^\mp)A'$  reaction on p-shell nuclei

FINUDA Collaboration

M. Agnello<sup>a</sup>, L. Benussi<sup>b</sup>, M. Bertani<sup>b</sup>, H.C. Bhang<sup>c</sup>, G. Bonomi<sup>p</sup>, E. Botta<sup>d</sup>, M. Bregant<sup>e</sup>, T. Bressani<sup>d</sup>, S. Bufalino<sup>g</sup>, L. Busso<sup>f</sup>, D. Calvo<sup>g</sup>, P. Camerini<sup>e</sup>, B. Dalena<sup>h</sup>, F. De Mori<sup>d</sup>, G. D'Erasmus<sup>h</sup>, F.L. Fabbri<sup>b</sup>, A. Feliciello<sup>g</sup>, A. Filippi<sup>g</sup>, E.M. Fiore<sup>h</sup>, A. Fontana<sup>i</sup>, H. Fujioka<sup>m</sup>, P. Genova<sup>i</sup>, P. Gianotti<sup>b</sup>, N. Grion<sup>j</sup>, V. Lucherini<sup>b</sup>, S. Marcello<sup>d</sup>, N. Mirfakhrai<sup>k</sup>, F. Moia<sup>p</sup>, P. Montagna<sup>i</sup>, O. Morra<sup>l</sup>, T. Nagae<sup>m</sup>, H. Ota<sup>n</sup>, A. Pantaleo<sup>o,1</sup>, V. Patocchio<sup>o</sup>, S. Piano<sup>j,\*</sup>, R. Rui<sup>e</sup>, G. Simonetti<sup>h</sup>, R. Wheadon<sup>g</sup>, A. Zenoni<sup>p</sup>

<sup>a</sup> Dip. di Fisica Politecnico di Torino, via Duca degli Abruzzi, Torino, and INFN Sez. di Torino, via P. Giuria 1, Torino, Italy<sup>b</sup> Laboratori Nazionali di Frascati dell'INFN, via E. Fermi 40, Frascati, Italy<sup>c</sup> Dep. of Physics, Seoul National Univ., 151-742 Seoul, South Korea<sup>d</sup> Dipartimento di Fisica Sperimentale, Università di Torino, via P. Giuria 1, Torino, and INFN Sez. di Torino, via P. Giuria 1, Torino, Italy<sup>e</sup> Dip. di Fisica, Univ. di Trieste, via Valerio 2, Trieste, and INFN, Sez. di Trieste, via Valerio 2, Trieste, Italy<sup>f</sup> Dipartimento di Fisica Generale, Università di Torino, via P. Giuria 1, Torino, and INFN Sez. di Torino, via P. Giuria 1, Torino, Italy<sup>g</sup> INFN Sez. di Torino, via P. Giuria 1, Torino, Italy<sup>h</sup> Dip. di Fisica Univ. di Bari, via Amendola 179, Bari, and INFN Sez. di Bari, via Amendola 179, Bari, Italy<sup>i</sup> INFN Sez. di Pavia, via Bassi 6, Pavia, Italy<sup>j</sup> INFN, Sez. di Trieste, via Valerio 2, Trieste, Italy<sup>k</sup> Dep. of Physics Shahid Beheshti Univ., 19834 Tehran, Iran<sup>l</sup> INAF-IFSI Sez. di Torino, C.so Fiume, Torino, and INFN Sez. di Torino, via P. Giuria 1, Torino, Italy<sup>m</sup> Dep. of Physics, Kyoto University, Kyoto 606-8502, Japan<sup>n</sup> RIKEN, Wako, Saitama 351-0198, Japan<sup>o</sup> INFN Sez. di Bari, via Amendola 179, Bari, Italy<sup>p</sup> Dip. di Meccanica, Università di Brescia, via Valotti 9, Brescia, and INFN Sez. di Pavia, via Bassi 6, Pavia, Italy

## ARTICLE INFO

## Article history:

Received 28 June 2011

Received in revised form 5 September 2011

Accepted 19 September 2011

Available online 24 September 2011

Editor: V. Metag

## ABSTRACT

This Letter is concerned with the study of the  $K_{stop}^- A \rightarrow \pi^\pm \Sigma^\mp A'$  reaction in p-shell nuclei, i.e.,  ${}^6\text{Li}$ ,  ${}^9\text{Be}$ ,  ${}^{13}\text{C}$  and  ${}^{16}\text{O}$ . The  $\pi^\pm \Sigma^\mp / K_{stop}^-$  emission rates are reported as a function of  $A$ . These rates are discussed in comparison with previous findings. The ratio  $\pi^- \Sigma^+ / \pi^+ \Sigma^-$  in p-shell nuclei is found to depart largely from that on hydrogen, which provides support for large in-medium effects possibly generated by the sub-threshold  $\Lambda(1405)$ . The continuum momentum spectra of prompt pions and free sigmas are also discussed as well as the  $\pi^\pm \Sigma^\mp$  missing mass behavior and the link with the reaction mechanism. The apparatus used for the investigation is the FINUDA spectrometer operating at the DAΦNE  $\phi$ -factory (LNF-INFN, Italy).

© 2011 Elsevier B.V. Open access under [CC BY license](http://creativecommons.org/licenses/by/3.0/).

## 1. Introduction

This Letter describes an experimental study of the reaction  $K_{stop}^- A \rightarrow \pi^\pm \Sigma^\mp A'$ , where  $A$  is  ${}^6\text{Li}$ ,  ${}^7\text{Li}$ ,  ${}^9\text{Be}$ ,  ${}^{13}\text{C}$  and  ${}^{16}\text{O}$ . In this study, the charged  $\Sigma$ -hyperons are reconstructed through their decay channels  $\Sigma^\pm \rightarrow n\pi^\pm$ . The requirement of having one neutron and two charged pions in the final state excludes charged  $\Sigma$ 's

and neutral  $\Lambda$ 's from the two-body absorption process  $K_{stop}^- 2N \rightarrow N\Sigma(\Lambda)$  since both final channels are characterized by a single pion. Moreover, the request for a final  $\Sigma$  excludes detection of the  $\Sigma$  conversion reaction,  $\Sigma N \rightarrow \Lambda N$ , and thus the identification of possible  $\Sigma$ -hypernuclear states. For these reasons, this measurement studies the elementary process  $K_{stop}^- p \rightarrow \pi^\pm \Sigma^\mp$  with the absorbing proton being embedded in  $A$ .

To understand the  $K^-$  nuclear and the  $Y$  nucleon(s) interactions, FINUDA pursued a program of  $K_{stop}^- A$  experimental studies through the methodical analysis of the reaction channels. This was to determine the  $A$ -dependence of  $\Lambda$  capture into hypernuclear bound states [1,2], which helped to constrain the threshold  $K^-$

\* Corresponding author. Fax: +39 040 5583350.

E-mail address: [stefano.piano@ts.infn.it](mailto:stefano.piano@ts.infn.it) (S. Piano).<sup>1</sup> Deceased.

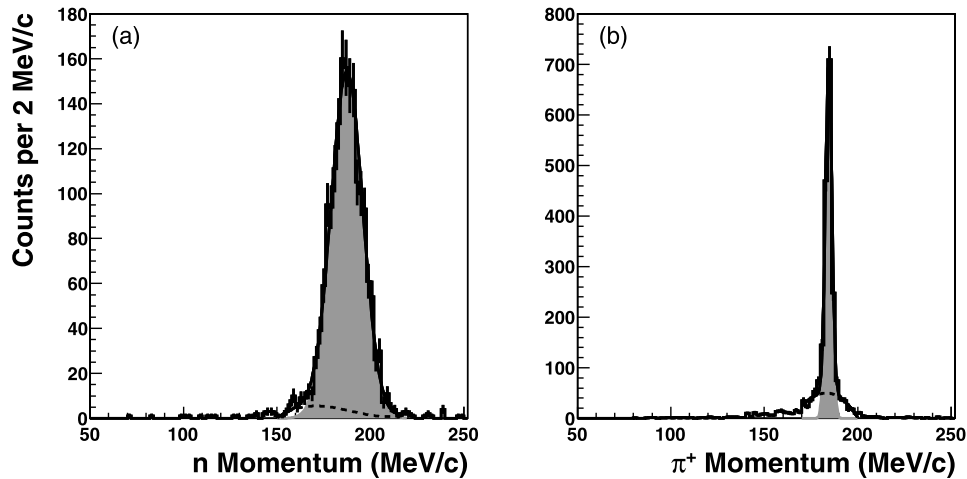


**Fig. 1.** Measured momentum distributions of neutrons and positive pions from positive sigma decays at rest,  $\Sigma^+ \rightarrow n\pi^+$ . The grey-filled peaks are the result of a Gaussian peak fitting, while the dotted lines are a polynomial best-fit to the background.

nuclear potential [3]. Study of the mesonic [4] and non-mesonic [5,6] weak decay of p-shell  $\Lambda$ -hypernuclei was also part of the  $K_{stop}^- A$  studies since it helps in understanding the  $\Lambda N$  weak interaction. The analyses of the pion-less  $K^-$  absorption leading to the selected  $\Lambda p$  [7],  $\Lambda d$  [8] and  $\Lambda t$  [9] channels established the possibility of  $K^-$ 's forming quasi-bound states. This is still a debated topic; however, it has spurred widespread interest [10]. The presence of nuclear matter may sensibly modify the sub-threshold behavior of the  $\bar{K}-N$  interaction depending on the nuclear density [11–14]. This occurrence may favorably be probed with the  $K_{stop}^- A \rightarrow \pi \Sigma A'$  reaction since the  $\pi \Sigma$  channel prevails over the other competing channels. Furthermore, the measurement involves a single proton bound in  $A$  and takes place at threshold, which also facilitates the study of the under-threshold behavior of the  $\bar{K}-N$  interaction.

Kaons, after stopping in nuclei, initially form K-atoms, leading to kaon absorption by nucleons lying at the nuclear surface, giving rise to a number of quasi-free reactions. This analysis selectively examines the  $K_{stop}^- p \rightarrow \pi^\pm \Sigma^\mp$  processes, where  $p$  is a bound proton. The prompt pion and free sigma momentum distributions describe the  $\pi$ - and  $\Sigma$ -continuum behavior in the reaction  $K_{stop}^- A \rightarrow \pi^\pm \Sigma^\mp A'$ . These spectra are discussed in detail rather than the  $\pi^\pm \Sigma^\mp$  invariant masses. In this case, the  $\pi \Sigma$  channel is filled by two resonances  $\Sigma(1385)$  and  $\Lambda(1405)$  as well as the  $\pi \Sigma$  continuum whose phase space develops in the same region as the two resonances [15]. The effects of  $\pi-A'$  and  $\Sigma-A'$  final-state interactions further complicate this scenario since they distort the initial shape of invariant mass distributions. The  $\pi$  ( $\Sigma$ ) momentum spectra may give a clearer picture of the dynamics of the  $K_{stop}^-$  absorption by a bound  $p$ . The  $\pi \Sigma$  missing mass spectra are discussed with the aim of measuring the energy lost via undetected particles. This is to investigate the number of nucleons involved in the kaon absorption and hence the reaction mechanism. The Letter also focuses on the  $\pi^\pm \Sigma^\mp / K_{stop}^-$  emission rates, which are compared to earlier bubble chamber measurements. Moreover, they are used to form the  $R_{+-}$  ratio (i.e.,  $\pi^- \Sigma^+ / \pi^+ \Sigma^-$ ) which is known to change significantly when moving the kaon absorption from a free proton to a bound proton [11–14].

## 2. The experimental procedure

All the particles involved in the  $A(K_{stop}^-, \pi^\pm \Sigma^\mp) A'$  reaction, i.e.,  $K^-$ 's (and correlated  $K^+$ 's),  $\pi^\pm$ 's and  $\Sigma^\mp$ 's (from  $n\pi^\mp$  de-

cays), are fully reconstructed. Negative and positive kaons result from decays of phi meson,  $\phi \rightarrow K^- K^+$  (BR  $\sim 50\%$ ),  $\phi$ 's produced by the  $e^+ e^- \rightarrow \phi(1020)$  reaction at the DAΦNE collider. The  $\phi$  mesons are created nearly at rest giving rise to kaon pairs which are emitted in nearly opposite directions with a kinetic energy of  $16.1 \pm 1.5$  MeV. The kaon pairs, after traversing the 2 inner layers of the spectrometer, stop in  $\sim 0.25$  gr/cm<sup>2</sup> thick targets about  $20.0 \times 5.3$  cm<sup>2</sup> in area. Most are solid slabs except for <sup>13</sup>C and <sup>16</sup>O, the first of which is carbon powder and the second liquid D<sub>2</sub>O. When a  $K^-$  starts the reaction, the  $K^- K^+$  pair triggers the inner layer of FINUDA and, simultaneously, a final-state particle must be detected by the outer layer of FINUDA. Such a selective trigger is mandatory to reject the overwhelming background originated by electrons and positrons circulating in DAΦNE.

The inner (TOFINO [16]) and outer (TOFONE [17]) sensitive layers of FINUDA are two segmented detectors made of plastic scintillator, which are organized as the staves of a barrel. The TOFINO barrel, which encloses the  $e^+ e^-$  interaction volume, has a diameter of 11 cm and is used for starting the time-of-flight system (*tof*) and for triggering purposes. TOFONE, which consists of 72 trapezoidal slabs 255 cm long and 10 cm thick, is the stop-counter of the FINUDA *tof*, which is used to determine the momentum of neutrons as well as for triggering purposes. The neutron momentum resolution of FINUDA is obtained from the distribution width of monokinetic neutrons arising from the decays of stopped positive sigmas. The momentum distribution of such neutrons is shown in Fig. 1(a), which displays a peak at  $187.6 \pm 0.2$  MeV/ $c$  and a width of  $8.4 \pm 0.2$  MeV/ $c$  at  $\sigma$ . This width is slightly narrower than the one reported in a previous analysis  $9.4 \pm 0.2$  MeV/ $c$  [18] due to a finer calibration of the present FINUDA *tof*. Neutrons from the first run of FINUDA cannot be utilized for this analysis because of the high threshold chosen for TOFONE, which was mainly used for triggering purposes. As a result, neutrons below 20 MeV were hardly detected and hence sigmas could not actually be reconstructed. The tracking system of FINUDA is located between TOFINO and TOFONE. It consists of a vertex detector [19], two intermediate layers of low-mass drift chambers [20] and an outer array of straw tubes [21]. The vertex detector comprises 2 layers of double-sided micro-strip silicon sensors [19] whose internal layer is located at about 7 cm from the trajectories of the  $e^+ e^-$  crossing beams. The 2 layers closely surround a stack of 8 solid targets. The outer six layers of straw tubes [21] have the inner layer set at 111.0 cm from the crossing beams. With the nominal field set at 1 T, the spectrometer is capable of analyzing  $184.5 \pm 0.1$  MeV/ $c$

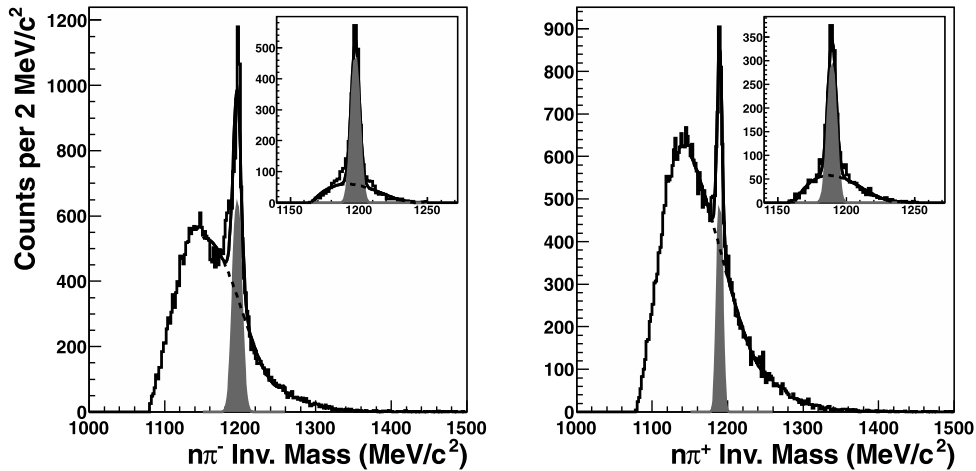


**Fig. 2.** Unconstrained  $n\pi^-$  and  $n\pi^+$  invariant mass distributions for the  ${}^6\text{Li}(K_{\text{stop}}^-, n\pi^\mp)A'$  reaction. The grey-filled peaks represent the  $\Sigma^-$  (left) and  $\Sigma^+$  signals. In the insets the constrained  $n\pi^\mp$  invariant mass distributions are shown. The applied constraints are detailed in the text.

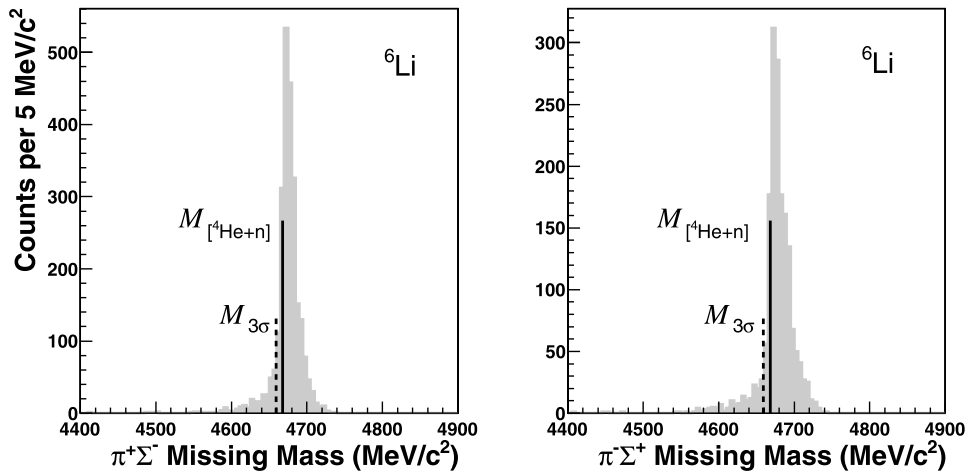


**Fig. 3.** Missing mass distribution for the  ${}^6\text{Li}(K_{\text{stop}}^-, \pi^\pm \Sigma^\mp)A'$  reactions. The full line denotes the physical threshold of the missing mass, the dotted line indicates the lower threshold chosen for the analysis.

positive pions with a resolution at  $\sigma$  of  $1.72 \pm 0.06$  MeV/c (see Fig. 1(b)), which only slightly worsens for pions of lower momenta. However, the reduced spectrometer resolution only weakly alters the continuous behavior of pion (and sigma) spectra.

In the present analysis, both kinematic and topological constraints are applied to measured observables. The primary condition for processing a  $n\pi^-\pi^+$  event requires a vertex in one of the targets between the trajectory described by the initial kaon pair and the track of one of the two final pions. A vertex position is reconstructed with an average spatial resolution of 0.7 mm, which is mostly due to the kaon straggling inside the target. In fact, the average resolution of the vertex detector in reconstructing a particle prong is 0.2 mm. The mass of a particle is then defined by the particle energy deposit ( $dE/dX$  technique) in the two layers of the vertex detector as well as in the two drift chambers. The  $dE/dX$  technique ensures an overall pion ID efficiency above 98%. Fig. 2 shows the  $n\pi^-$  and  $n\pi^+$  invariant mass behaviors for  ${}^6\text{Li}$ . The sharp peaks identify the  $\Sigma^\mp$  signals, which are placed at  $1197.0 \pm 3.4(\sigma)$  MeV/ $c^2$  and  $1189.2 \pm 3.5(\sigma)$  MeV/ $c^2$ , respectively. The signal to background ratio assigned by a peak-fitting procedure is  $(S/B)_{\Sigma^-} = 1.0$  and  $(S/B)_{\Sigma^+} = 0.7$ , where  $S$  is the area of the grey-filled peaks taken at  $2\sigma$  and  $B$  is the area below the dotted curves taken in the same mass range. For these spectra, the background  $B$  is mostly due to gammas which may emulate neu-

trons in TOFONE, and by neutrons which may scatter before being detected. The background due to misidentification of pions is negligible. A clear background reduction is obtained by requiring the kinematic observables of the  $n\pi^\mp$  events to belong to the phase space volume of the  $\Sigma^\mp \rightarrow n\pi^\mp$  decays, which safely includes the prompt pions. As an example, when applying the above phase space constraints to  $n\pi^\mp$  events, the  $n\pi^-$  and  $n\pi^+$  invariant mass distributions are dominated by  $\Sigma^-$  and  $\Sigma^+$  peaks, see the insets of Fig. 2. When peak fitting these distributions (  $(S/B)_{\Sigma^-} = 4.5$  and  $(S/B)_{\Sigma^+} = 3.6$  thereby permitting a reliable discussion of the  $\Sigma$  physics.

### 3. The results

Prompt pions and free sigmas (see Fig. 2 and related discussion) are fully reconstructed, which ensures a quasi-exclusive character to this measurement. Accordingly, the observables involved in the  $\pi^\pm \Sigma^\mp$  analysis, i.e., missing masses, momentum distributions and emission rates, should be scarcely affected by background. Fig. 3 shows the  $(K_{\text{stop}}^-, \pi^\pm \Sigma^\mp)$  missing mass ( $M$ ) spectra of  ${}^6\text{Li}$ . These spectra are formed with the same data set of the constrained  $n\pi^\pm$  invariant masses, i.e., the grey-filled distributions in the insets of Fig. 2. The full line denotes the physical threshold of the missing mass, that is, the value acquired by  $M$  when  $A' \equiv [{}^4\text{He}_{g.s.} + n]$ .

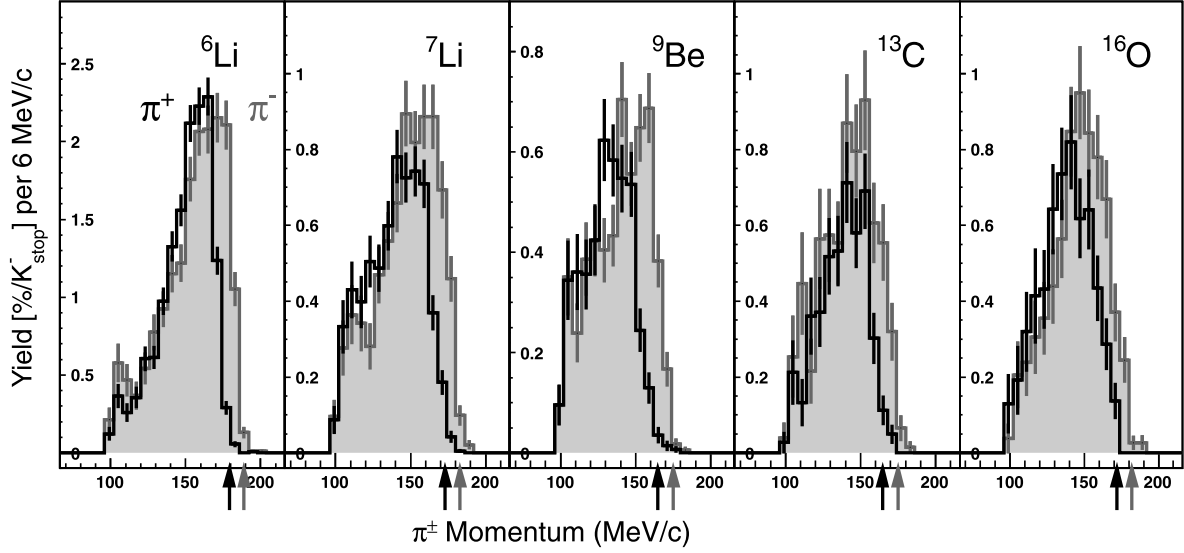


**Fig. 4.** Measured momentum distributions of prompt pions from the  $A(K_{stop}^-, \pi^\pm \Sigma^\mp)A'$  reactions. The open (grey-filled) histograms describe the behavior of positive (negative) pions and the black (grey) arrows point to the  $p[B_{\Sigma^{-(+)}} = 0]$  threshold.

The dotted line points to the missing mass threshold ( $M_{3\sigma}$ ) used in this analysis, where the overall uncertainty in measuring  $M$  is  $\sigma = 3.1$  MeV/ $c^2$ , or a full-width at half-maximum FWHM = 7.3 MeV/ $c^2$ . Both distributions are peaked at about 10 MeV/ $c^2$  above  $M_{[{}^4\text{He}+n]}$  and have a FWHM in the range 22–24 MeV/ $c^2$ .

Fig. 4 shows the measured momentum distributions of prompt pions from the  $K_{stop}^- A \rightarrow \pi^\pm \Sigma^\mp A'$  reactions. The arrows denote the condition  $p[B_{\Sigma^{-(+)}} = 0]$ , where  $B_\Sigma$  is the binding energy of possible  $\Sigma$ -hypernuclei ( ${}_\Sigma A$ ). Therefore, broad peaks arising at  $p[B_{\Sigma^{-(+)}} > 0]$  would disclose the presence of  ${}_\Sigma A$  states. Such states cannot be observed in the present spectra since they are inhibited by requiring a  $\Sigma$  to be present in the reaction exit channel. The distributions of pion (sigma in Fig. 5) momenta are corrected for the spectrometer acceptance, which is the largest source of systematic uncertainty. Such corrections relied on a Monte Carlo code which embodied the FINUDA geometry. The code was required to generate  $K_{stop}^- A \rightarrow \pi^+ \pi^- n A'$  events with the final particles distributed uniformly over a range of momenta required by the reaction kinematics. The generated events fully crossing the geometry of FINUDA were finally reconstructed with the analysis code. The ratio of the reconstructed to generated events defines the acceptance of the apparatus. For a selected momentum bin, the systematic uncertainty of the acceptance results from the statistical uncertainty of the reconstructed events and the systematic uncertainty arising from the reconstruction of real events, the two uncertainties being added in quadrature. Finally, the error bars associated with the data-points in Figs. 4 and 5 account for the statistics of real events and systematic uncertainty of the acceptance, again calculated by summing in quadrature the two uncertainties. The pion threshold of the spectrometer is slightly below 80 MeV/ $c$ ; however, the pion momentum distributions are cut at 100 MeV/ $c$  to avoid large bin fluctuations due to acceptance correction. Note that above the  $p[B_{\Sigma^{-(+)}} = 0]$  thresholds the spectra are scarcely affected by background. The momenta of  $\Sigma^\pm$ 's are determined by measuring the momenta of their decay products. For  ${}^6\text{Li}$ , the measured momentum distributions of  $\Sigma^\pm$ -hyperons are shown in Fig. 5 (grey-filled histograms). For  $\Sigma^-$ , the distribution resembles a rather symmetric bump peaked at about 165 MeV/ $c$  with a FWHM of 155 MeV/ $c$  and shows no strength at around 0 MeV/ $c$ . The  $\Sigma^+$  momentum distribution is instead peaked at around 0 MeV/ $c$  and a 160 MeV/ $c$  broad-bump arises at  $\sim 174$  MeV/ $c$ . In this case,

the FWHM of the bump is assessed by removing via a global-fitting method the 0 MeV/ $c$  peak, which ultimately smears out the line-shape of the bump. The  $\Sigma^\pm$  bumps display little variation in shape: the  $\sim 10$  MeV/ $c$  peak shift is explained by the different sigma masses, while the  $\sim 5$  MeV/ $c$  wider bump of the  $\Sigma^+$ -hyperons is well within the uncertainties in assessing the  $\Sigma^\pm$  bump widths. For the other nuclei, the  $\Sigma^\pm$  momentum distributions are not shown since they display shapes similar to the  $\Sigma^\pm$  momentum distributions of  ${}^6\text{Li}$  with the only exception being the number of  $\Sigma^+$  events in the 0 MeV/ $c$  peak, which basically depends on the target size and density. Such a behavior suggests a way for representing all the  $\Sigma^\pm$  measured momentum distributions, which is based on the fact that their symmetric line-shapes can be fitted by means of Gaussian functions. With this approach, the  $\Sigma^+$  momentum distributions are found to have a mean value of  $167 \pm 7$  MeV/ $c$  and a FWHM  $178 \pm 20$  MeV/ $c$ , and the  $\Sigma^-$  momentum distributions a mean value of  $157 \pm 11$  MeV/ $c$  and a FWHM  $161 \pm 9$  MeV/ $c$ .

The sigma momentum distributions appear rather dissimilar at around 0 MeV/ $c$ . At these momenta, positive and negative sigmas behave differently when traveling through nuclear targets of finite thickness. For example, a  $\Sigma^+$  can stop in a target without being absorbed by a surrounding nucleus, which explains the appearance of the peak at around 0 MeV/ $c$ . When a  $\Sigma^-$  comes to rest, it is captured by a target nucleus and later undergoes a  $\Sigma^- A$  conversion.  $\Lambda$ -hyperons are not presently reconstructed hence the momentum distribution shows no strength at around 0 MeV/ $c$ . To account for the different behavior of low-energy charged sigmas in targets of finite size, a Monte Carlo code was developed which employs the  $K_{stop}^- A \rightarrow \pi^\pm \Sigma^\mp A'$  quasi-free reaction to generate the sigma momentum spectra. Then, the spectra were filtered through the geometry of FINUDA, which also accounts for the interaction of  $\Sigma^\mp$  with the target media. The resulting momentum spectra (open histograms) are finally compared with the measured momentum spectra and show a reasonable overall agreement. The Monte Carlo generated  $\Sigma^\mp$  momentum spectra are displayed in Fig. 5 with full dots.

The  $K_{stop}^- A$  emission rate leading to final  $\pi \Sigma$  pairs is defined by the ratio:

$$R_A = \frac{N_{\pi \Sigma}}{N_{K_{stop}^-}} \quad (1)$$

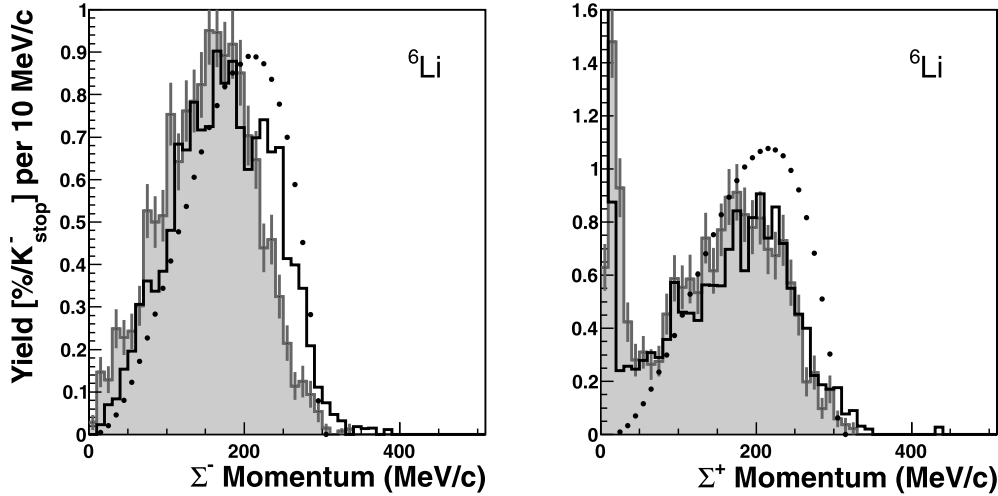


**Fig. 5.** Momentum distributions of sigmas from the  ${}^6\text{Li}(K_{\text{stop}}^-, \pi^\pm \Sigma^\mp)A'$  reactions. The grey-filled histograms are the measured distributions. The distributions of Monte Carlo generated sigmas are depicted by full dots, and with open diagrams are represented the Monte Carlo generated sigmas being reconstructed by FINUDA.

**Table 1**  
The table lists  $R_A$  for  $\pi^- \Sigma^+$  and  $\pi^+ \Sigma^-$  as a function of  $A$ , where  $R_A$  is given in units of  $[10^{-2}/K_{\text{stop}}^-]$ . The  $R_A$  values are followed by the statistical and systematic uncertainties.  $\Sigma_{\text{loss}}^-$  is expressed in units of [%]. The emission rates of  ${}^4\text{He}$  and  ${}^{12}\text{C}$  are taken from Refs. [22] and [23], respectively.  $R_{+-} = R_A(\pi^- \Sigma^+)/R_A(\pi^+ \Sigma^-)$ .

A	$R_A$		$\Sigma_{\text{loss}}^-$	$R_{+-}$
	$\pi^- \Sigma^+$	$\pi^+ \Sigma^-$		
${}^4\text{He}$	$12.8 \pm 2.4$	$7.2 \pm 1.4$	–	$1.8 \pm 0.5$
${}^6\text{Li}$	$17.6 \pm 1.0 \pm 1.3$	$14.4 \pm 1.1 \pm 0.2$	$30 \pm 2$	$1.2 \pm 0.1 \pm 0.1$
${}^7\text{Li}$	$7.8 \pm 0.5 \pm 0.2$	$6.4 \pm 0.4 \pm 0.6$	$26 \pm 2$	$1.2 \pm 0.1 \pm 0.1$
${}^9\text{Be}$	$5.5 \pm 0.3 \pm 0.3$	$4.3 \pm 0.2 \pm 0.5$	$38 \pm 3$	$1.3 \pm 0.1 \pm 0.2$
${}^{12}\text{C}$	$9.2 \pm 0.3$	$7.3 \pm 0.2$	–	$1.25 \pm 0.09$
${}^{13}\text{C}$	$6.8 \pm 0.8 \pm 0.6$	$4.6 \pm 0.5 \pm 0.2$	$12 \pm 1$	$1.5 \pm 0.2 \pm 0.1$
${}^{16}\text{O}$	$6.9 \pm 0.6 \pm 0.3$	$5.8 \pm 0.5 \pm 0.2$	$36 \pm 3$	$1.2 \pm 0.1 \pm 0.1$

where  $N_{\pi\Sigma}$  is the number of  $\pi\Sigma$  pairs produced when  $N_{K_{\text{stop}}^-}$  negative kaons stop in  $A$ . These two observables can be related to the number of  $\pi\Sigma$  ( $N_{\pi\Sigma}^{\text{CE}}$ ) and  $K_{\text{stop}}^-$  ( $N_{K_{\text{stop}}^-}^{\text{CE}}$ ) counted events (CE) through the equations:

$$N_{\pi\Sigma} = \frac{N_{\pi\Sigma}^{\text{CE}}}{\epsilon_{\pi\Sigma}} \quad \text{and} \quad N_{K_{\text{stop}}^-} = \frac{N_{K_{\text{stop}}^-}^{\text{CE}}}{\epsilon_{K_{\text{stop}}^-}} \quad (2)$$

where the parameters  $\epsilon$  correct the observables  $N_{\pi\Sigma}^{\text{CE}}$  and  $N_{K_{\text{stop}}^-}^{\text{CE}}$  for instrumental flaws, namely, the apparatus finite acceptance, inability to fully reconstruct all the  $n\pi^\pm$  events, misidentification of particles and trigger inefficiencies. Both  $\epsilon_{\pi\Sigma}$  and  $\epsilon_{K_{\text{stop}}^-}$  are assessed with standard Monte Carlo techniques. A second partially-independent approach to calculate both  $N_{\pi\Sigma}$  and  $N_{K_{\text{stop}}^-}$  is also available, which requires a muon from  $K^+ \rightarrow \mu^+ \nu_\mu$  (BR = 63.6%) in coincidence with the  $n\pi^+\pi^-$  initial event. Such an approach avoids any trigger inefficiency but also reduces the useful data-set by at least BR, which causes the statistical uncertainties to augment. When taken with their overall uncertainties, these emission rates are consistent with those calculated by using Eq. (1), so only  $R_A$ 's are reported in Table 1.

The  $R_A$  values are listed with their statistical and systematic uncertainties those listed in the  $\pi^+ \Sigma^-$  column account for the  $\Sigma^-$  loss ( $\Sigma_{\text{loss}}^-$ ) at momenta around 0 MeV/c. For a given nucleus,  $\Sigma_{\text{loss}}^-$  is calculated as follows: by using the momentum distribution of positive sigmas, a loss rate is initially defined by the ratio of the number of sigmas in the 0 MeV/c peak to the number of sigmas in the bump. The number of sigmas in the 0 MeV/c peak as well as in the bump is determined by a global best-fit analysis, where the bump is assumed to have a Gaussian line-shape. Then, the loss rate

of positive sigmas is assigned to negative sigmas. As a final note, the  $R_A$  data-set is not corrected for the pion attenuation in  $A'$  nor for the  $\Sigma-A$  conversion; therefore, these observables represent the emission rates of the reaction  $A(K_{\text{stop}}^-, \pi^\pm \Sigma^\mp)A'$ . In column five the  $R_{+-}$  ratio (the ratio between  $R_A(\pi^- \Sigma^+)$  and  $R_A(\pi^+ \Sigma^-)$ ) is reported.

Table 1 also gives an account of the rates published by earlier bubble chamber measurements, the emission rates of  ${}^4\text{He}$  [22] and the capture rates of  ${}^{12}\text{C}$  [23]. For the purpose of comparison, the  ${}^{12}\text{C}$  capture rates are reduced to emission rates by means of the numbers discussed in Ref. [23]. In this article,  $R_{12\text{C}} = 12.7$  (15.9) for the  $\pi^+ \Sigma^-$  ( $\pi^- \Sigma^+$ ) channel, which becomes 7.9 (9.9) when the  $\Sigma-A$  conversion is neglected and finally 7.3 (9.2) when the pion-flux attenuation is not taken into account. The ratio between the emission and capture rates  $\pi^- \Sigma^+ / \pi^+ \Sigma^-$  remains the same  $1.25 \pm 0.09$ . The same data on carbon are reanalyzed in a second article [24], which calculates the capture rates for some  $\pi\Sigma$  channels. In this article, a capture rate  $0.131 \pm 0.004$  for  $\pi^+ \Sigma^-$  was found (about the same as in the first article) and  $0.294 \pm 0.010$  for  $\pi^- \Sigma^+$  (about twice the value previously published) resulting in the ratio  $2.24 \pm 0.12$  [24]. Such a large value of the capture rate for  $\pi^- \Sigma^+$  is however based on an emission rate of 9.3, a value that can be assessed via the number of events reported in Table I of Ref. [24]. Such a value is in close agreement with 9.2 the value given in Table 1.

#### 4. Discussion and conclusions

The analysis aimed at examining the elementary process  $K_{\text{stop}}^- p \rightarrow \pi^\pm \Sigma^\mp$  with  $p$  belonging to  $A$ . The experimental method



of searching for  $\pi\Sigma$  pairs relies on the capability of FINUDA to detect all the particles involved in the  $K$  absorption process, i.e.,  $K_{stop}^-$  (and the associated  $K^+$ ),  $\pi^\pm$  and  $n$ . For  ${}^6\text{Li}$ , this method assigns a signal-to-background ratio to sigmas (detected in coincidence with pions) of  $(S/B)_{\Sigma^+} = 3.6$  and  $(S/B)_{\Sigma^-} = 4.5$ . The other targets show similar ratios.

Fig. 3 shows that the  $\pi^\pm\Sigma^\mp$  missing mass distributions are 22–24 MeV/ $c^2$  FWHM. These widths are only in part explained by the measurement uncertainty. When accounting for the instrumental uncertainty, FWHM = 7.3 MeV/ $c^2$ , the missing mass strength is mostly found in the range  $\sim 10 \pm 11$  MeV/ $c^2$ , where  $\sim 10$  MeV/ $c^2$  is the  $M$  peak position above the  $M_{[{}^4\text{He}+n]}$  threshold and  $\pm 11$  MeV/ $c^2$  FWHM is the intrinsic width of the distribution. This missing energy must be compared with the available energy, the kaon rest mass, to realize that the  $\pi^\pm\Sigma^\mp$  final pairs take away from 96% to 100% of the energy available to the reaction. The fraction of energy lost is below 4%, which can be explained by the energy subtracted by de-excitation  $\gamma$ 's or by unobserved fragments of  $A'$  as well as by the energy lost by sigmas when traveling through a target. This trait establishes the quasi-free nature of the reaction. Such a valuation also indicates that the  $\pi\Sigma$  kinematics is only slightly altered by final-state interactions. The above discussion is related to  ${}^6\text{Li}$  but similar conclusions can also be drawn for the other nuclei,  ${}^7\text{Li}$ ,  ${}^9\text{Be}$ ,  ${}^{13}\text{C}$  and  ${}^{16}\text{O}$ . In fact, the missing mass distributions (figures not shown) broaden out to a maximum of 20% when going from  $A = 6$  to  $A = 16$ .

The  $\pi^\pm\Sigma^\mp$  data discussed in this Letter are the result of an exclusive measurement, more than 96% of the available energy is in fact taken by  $\pi\Sigma$  pairs. Previous results were obtained from either studies of inclusive measurements on  ${}^4\text{He}$  [25] and  ${}^{12}\text{C}$  [26] or semi-inclusive measurements on a variety of nuclei [27]. For this other class of measurements, there are several processes leading to the same final state; in Ref. [27], the  $\pi^-$  momentum spectrum induced by the  $(K_{stop}^-, \pi^-)$  reaction is decomposed into six different processes, which makes the separation of the  $(K_{stop}^-, \pi^- \Sigma^+)$  process from the others difficult.

Fig. 4 shows the momentum spectra of prompt pions, which exhibit a continuum behavior from the kinematic threshold down to 100 MeV/ $c$ . These spectra are not corrected for the pion attenuation. Above the kinematic threshold (indicated by arrows in Fig. 4), the  $\pi^\pm$  momentum spectra are seen to be nearly unaffected by background. The pion spectra are not compared with theoretical predictions, although the absorption of at-rest kaons in nuclei is addressed in Ref. [28]. The authors develop a plain model of the interaction, which is only capable of explaining the shape of the spectra without helping the interpretation of the data presently discussed. The similarity among the measured momentum distributions of sigmas shows that the  $K_{stop}^- A$  absorption reaction depends weakly on  $A$  for p-shell nuclei. This is also corroborated by the analyses based on Monte Carlo simulations, which show that the quasi-free reaction  $K_{stop}^- A \rightarrow \pi\Sigma A'$  is capable of explaining the shapes of all the distributions. Moreover, the sigma momentum spectra are weakly distorted by  $\Sigma-A$  final-state interactions since they mainly proceed via the  $\Sigma N \rightarrow \Lambda N$  conversion reaction, which selectively removes sigmas from the outgoing flux. Therefore, the Monte Carlo generated sigma momentum distributions (full dots in Fig. 5) give a fair account of the shapes of sigma momenta. The  $\Sigma$  to  $\Lambda$  conversion rate was not determined for these spectra.

The emission rates  $\pi^\pm\Sigma^\mp/K_{stop}^-$  are reported in Table 1. They are also compared with earlier bubble chamber measurements for  ${}^4\text{He}$  [22] and  ${}^{12}\text{C}$  [23], which were published in the early seventies. To this day, these are the only available data. When the  $K_{stop}^- p \rightarrow \pi^\pm\Sigma^\mp$  elementary process occurs on a bound proton the relationship  $R_{+-} > 1$  holds for light nuclei; in fact, the  $R_{+-}$  ratio

ranges from 1.8 to 1.3 to 1.2 for  ${}^4\text{He}$ ,  ${}^9\text{Be}$  and  ${}^{16}\text{O}$ , respectively. If the same process occurs on a free proton ( $H$ ) then the relationship is reversed:  $R_{+-} = 0.42$  ( $\gamma^{-1}$  in Ref. [29]). Such a clear increase of  $R_{+-}$ , when moving the interaction from a free proton to a bound proton, can be related to the sub-threshold modification of the  $\bar{K}N$  interaction.

For the light nuclei examined, the average value of  $R_{+-}$  is  $1.3 \pm 0.1$  whose flat behavior indicates that the kaon absorption occurs preferentially at the surface of a nucleus. This value of  $R_{+-}$  can be compared directly with the ratio  $R_{+-} = \text{Yield } \pi^- \Sigma^+ / \text{Yield } \pi^+ \Sigma^-$  being calculated in Ref. [11]. In this article, the behavior of  $R_{+-}$  is given as a function of  $\rho/\rho_0$ , where  $\rho_0$  is the nuclear density at saturation.  $R_{+-}$  is predicted to vary from 1.4 to 1.7 for  $\rho/\rho_0$  ranging from 0.0 to 0.35, this range accounting for the nuclear skin densities of light nuclei. Moreover, the ratio  $R_{+-}$  corresponds to the model  $c$  option, that is, the option that accounts for final-state particle absorption. The agreement between theoretical predictions and the experimental value of  $R_{+-}$  is remarkable. The discussion on the measured emission rates cannot take further advantage of the comparison with theory because of the lack of model calculations. The exception is the inclusive reaction  ${}^{12}\text{C}(K_{stop}^-, \pi^\pm)$ , where capture rates as well as pion momentum spectra are calculated [13].

The absorption of stopped kaons involves only surface protons when the final-state particles are  $\pi^\pm\Sigma^\mp$  pairs. Nevertheless, Table 1 shows that when a neutron is added to a nucleus  $R_A$  drops for both channels; in fact, for the lithium isotopes is  $R_{7\text{Li}}/R_{6\text{Li}} = 0.44$  for both  $\pi^- \Sigma^+$  and  $\pi^+ \Sigma^-$ . This fact reflects the excess of surface neutrons over surface protons of  ${}^7\text{Li}$  with respect to  ${}^6\text{Li}$ . Such an excess has the net effect of depleting the number of  $K^- A$  stop centers leading to  $\pi^\pm\Sigma^\mp$  pairs. The same relationship is also found for the carbon isotopes,  $R_{13\text{C}}/R_{12\text{C}} = 0.75$  for  $\pi^- \Sigma^+$  and 0.63 for  $\pi^+ \Sigma^-$ . As a final note, the large values of  $R_A$ 's found for  ${}^6\text{Li}$  reflect the previously measured large value for  ${}^4\text{He}$  since this nucleus forms the lithium core.

## Acknowledgements

This work was supported by the Istituto Nazionale di Fisica Nucleare (INFN) of Italy. It is a pleasure to thank Prof. A. Gal for the useful suggestions. The support received from the DAΦNE crew was indispensable for the success of the experiment, which was highly appreciated.

## References

- [1] M. Agnello, et al., Phys. Lett. B 622 (2005) 53.
- [2] M. Agnello, et al., Phys. Lett. B 698 (2011) 219.
- [3] A. Cieply, et al., Phys. Lett. B 698 (2011) 226.
- [4] M. Agnello, et al., Phys. Lett. B 681 (2009) 139.
- [5] M. Agnello, et al., Nucl. Phys. A 804 (2008) 151.
- [6] M. Agnello, et al., Phys. Lett. B 685 (2010) 247.
- [7] M. Agnello, et al., Phys. Rev. Lett. 94 (2005) 212303.
- [8] M. Agnello, et al., Phys. Lett. B 654 (2007) 80.
- [9] M. Agnello, et al., Phys. Lett. B 669 (2008) 229.
- [10] W. Weise, Nucl. Phys. A 835 (2010) 51;  
A. Gal, Prog. Theor. Phys. Suppl. 186 (2010) 270.
- [11] S. Wycech, Nucl. Phys. B 28 (1971) 541.
- [12] L.R. Staronski, S. Wycech, J. Phys. G 13 (1987) 1361.
- [13] A. Ohnishi, Y. Nara, V. Koch, Phys. Rev. C 56 (1997) 2767.
- [14] E. Friedman, A. Gal, Phys. Rep. 452 (2007) 89.
- [15] D. Jido, E. Oset, T. Sekihara, Eur. Phys. J. A 47 (2011) 42.
- [16] V. Filippini, M. Marchesotti, C. Marciano, Nucl. Instrum. Methods A 424 (1999) 343.
- [17] A. Pantaleo, et al., Nucl. Instrum. Methods A 545 (2005) 593.
- [18] M. Agnello, et al., Phys. Lett. B 701 (2011) 556.
- [19] P. Botton, et al., Nucl. Instrum. Methods A 427 (1999) 423.
- [20] M. Agnello, et al., Nucl. Instrum. Methods A 385 (1997) 58.

- [21] L. Benussi, et al., Nucl. Instrum. Methods A 361 (1995) 180;  
L. Benussi, et al., Nucl. Instrum. Methods A 419 (1998) 648.
- [22] P.A. Katz, et al., Phys. Rev. D 1 (1970) 1267.
- [23] C. Vander Velde-Wilquet, et al., Nucl. Phys. A 241 (1975) 511.
- [24] C. Vander Velde-Wilquet, et al., Nuovo Cimento 39A (1977) 538.
- [25] T. Harada, T. Akaishi, Phys. Lett. B 262 (1991) 205.
- [26] P.C. Gugelot, S.M. Paul, R.D. Ransome, Phys. Rev. C 41 (1990) 2445.
- [27] H. Ota, et al., Prog. Theor. Phys. Suppl. 117 (1994) 177.
- [28] C.B. Dover, D.J. Millener, A. Gal, Phys. Rep. 184 (1989) 1.
- [29] R.J. Nowak, et al., Nucl. Phys. B 139 (1978) 61.